

CFD modelling of fall pipe rock dumping using PICIN

Qiang CHEN¹, David M KELLY^{2,3}, Jeremy SPEARMAN²,
Aggelos DIMAKOPOULOS², Jun ZANG¹, Chris J K
WILLIAMS¹

¹ Department of Architecture and Civil Engineering, University of Bath, BA2 7AY. q.chen@bath.ac.uk; j.zang@bath.ac.uk; c.j.k.williams@bath.ac.uk

² HR Wallingford, Howbery Park, Wallingford, Oxfordshire, OX10 8BA, UK. dakelly@fiu.edu; j.spearman@hrwallingford.com;
a.dimakopoulos@hrwallingford.com

³ International Hurricane Research Center, Florida International University, Miami FL 33199, USA. dakelly@fiu.edu

Presented at Coastal Sediments 2015, San Diego, California, USA, 11 - 15 May 2015

Abstract

In this paper fall pipe rock dumping is investigated in 2D using the PICIN CFD model. PICIN employs the hybrid Eulerian-Lagrangian full particle Particle-In-Cell framework for incompressible free surface flow augmented with a full two-way fluid-solid interaction model. The PICIN model is first compared against a benchmark case of two circular particles falling in a water-filled tube. The results agree well with the numerical predictions of Patankar (2001). When applied to cases of randomly shaped rocks falling in pipe, the PICIN model seems to capture the physical processes and mechanisms that lead to clustering of the rocks.

Introduction

The targeted placement of rock onto the sea bed is a common solution for the protection of offshore pipelines and cables and scour protection for windfarm structures. In deeper waters (50m or more) to ensure the accuracy of this placement, rock is dumped via a fall-pipe - a long, vertical, semi-open, flexible fall pipe of typically around 1 m in diameter. Usually the pipe consists of a string of bottomless, heavy buckets which extends from the work vessel to a position just above the seabed where the material is to be placed (IADC 2012). Rock (typically several inches in diameter) is placed into the top of the pipe from a conveyor belt (at rates of up to 2000 tonnes/hour) and this material exits the pipe over the required location. The fall-pipes may be up to a thousand meters long. Because of the open structure of the flexible fall-pipe, water is able to enter the pipe and the falling rock causes a downwards directed water flow and a reduction in pressure in the pipe (Ravelli 2012). In some cases this pressure reduction can lead to pipe failure and considerable delay and cost. This behaviour can be further complicated by the interaction of the rocks themselves. Rock fall-pipes display clumping behaviour depending on the volume concentration, which is common to many granular systems in pipes (e.g. Raafat et al. 1996; Nakahara and Isoda 1997; Bertho et al. 2002). This clumping behaviour may contribute to the failure of pipes and represents a limiting factor on productivity.

This paper outlines the development and application of a state-of-the-art numerical model as a starting point in order to attempt to capture the physical processes occurring in rockfall pipes. The ultimate goal of this research being to develop a basis for optimization and improvement of rock fall productivity. The numerical model described is the Particle-In-Cell INcompressible (PICIN) model developed jointly by the University of Bath and HR Wallingford. PICIN is a full Navier-Stokes solver for incompressible free surface flows. The model is capable of full two-way fluid-solid interaction using the Distributed Lagrange Multiplier (DLM) approach of Patankar (2001). For the fluid phase the model uses a hybrid Eulerian-Lagrangian approach. The velocity field is updated on the grid by solving the governing equations, while particles, initially seeded inside the calculation grid, are used to track the free surface and advect the fluid and solid velocity fields. Moreover, for enhanced accuracy, the Dirichlet boundary condition for (zero) pressure is applied exactly at the free surface via a level set type approach. Solids are modelled as being initially fluid, a density correction is then made and the rigidity constraint is finally enforced using a rigidity maintaining force as the Lagrange multiplier. This is similar to the way that fluid incompressibility is enforced in projection type Navier-Stokes solvers using the pressure as the Lagrange multiplier. It is noted that this approach for fluid solid coupling implicitly conserves mass and momentum. This formulation leads to a no-slip condition at fluid-solid boundaries. In the work presented here the multiple solid-solid interactions are handled using the collision model of Glowinski et al. (1999) augmented with the multi-sphere Discrete Element method (DEM) suggested by Favier et al. (1999). This paper is organized as follows: the next section provides a summary of the governing equations and the numerical approach employed to solve them. Section 3 then provides a validation case in the form of two solid particles interacting as they fall through a tube of water with a free surface. In section 4 an example simulation of rocks falling through a pipe in two spatial dimensions is presented. Finally, in section 5 conclusions are drawn and further work on the topic is suggested.

1. The PICIN CFD model

1.1. Governing equations

The governing equations used for Newtonian fluid with free surface and two-way fluid-solid interactions in PICIN can be written as:

$$\Delta \cdot \mathbf{u} = 0 \quad \text{in } \Omega, \quad (1)$$

$$Du[\mathbf{u}] = 0 \quad \text{in } \Omega_S, \quad (2)$$

$$\frac{\partial \mathbf{u}}{\partial t} + (\mathbf{u} \cdot \nabla) \mathbf{u} = \mathbf{f} - \frac{1}{\rho} \nabla p + \nu \Delta^2 \mathbf{u} \quad \text{in } \Omega_F, \quad (3)$$

$$\frac{\partial \mathbf{u}}{\partial t} + (\mathbf{u} \cdot \nabla) \mathbf{u} = \mathbf{f} - \frac{1}{\rho_S} \nabla p + \nu \Delta^2 \mathbf{u} \quad \text{in } \Omega_S, \quad (4)$$

With the boundary conditions:

$$\mathbf{u} = \mathbf{u}_r(t) \quad \text{on } \partial\Omega \quad (5)$$

and:

$$\mathbf{u} = \mathbf{u}_i \quad (\mathbf{\Pi} - p\mathbf{I}) \cdot \mathbf{n} = \mathbf{T} \quad \text{on } \partial\Omega_S(t) \quad (6)$$

where Ω , Ω_S and Ω_F are the overall computation domain, solid phase and fluid phase, respectively; $\partial\Omega_S$ and $\partial\Omega$ are the solid/fluid interface and the domain boundaries, respectively; \mathbf{u} represents the velocity field; p is the pressure field; ν accounts for the dynamic viscosity of the fluid; ρ and ρ_S are the fluid density and solid density, respectively and \mathbf{f} is an external force. The governing equations for the solid phase (Eq. 2 and Eq. 3) are similar to the ones for the fluid phase (Eq. 1 and Eq. 4) except that viscosity term in the solid momentum equation (Eq. 3) is omitted due to the rigid body constraint (Eq. 2). This constraint ensures a rigid body motion and gives rise to an extra deformation stress tensor $\mathbf{\Pi}$, in addition to the pressure field. Alternatively, $\mathbf{\Pi}$ can be considered as a Lagrange multiplier that arises due to the rigid body constraint (Patankar et al. 2000). Eq. 6 gives a non-slip solid boundary condition at the solid/fluid interface, where \mathbf{T} is the traction force of the fluid to the solid, \mathbf{n} is the normal vector of solid surface and \mathbf{I} is an identity matrix. We note that this boundary equation will be implicitly handled within the DLM scheme.

As a hybrid method, PICIN divides the solution into two major steps: an Eulerian step and a Lagrangian step. Particles are initially seeded inside the underlying staggered Cartesian grid (see e.g. Harlow and Welch 1965), where 4 particles are used for each full fluid cell in 2D. The main idea is that during the Eulerian step the governing equations are solved on the grid at each time step to update the velocity field, which is then advected by the particles in a Lagrangian manner. A bilinear interpolation in 2D is used to map the new divergence free velocity field onto particles, and after the velocity field is advected it will be transferred back to the grid for next time step calculation.

1.2. The Eulerian step

In the Eulerian step the fluid motion is solved using the pressure projection technique of Chorin (1968). The external force and viscosity diffusion term are sequentially used to calculate a tentative velocity field \mathbf{u}_t by means of an explicit Euler time-advancing scheme. Subsequently, the velocity at the next time step can be derived from the tentative velocity and the pressure gradient as shown in Eq. 7 using an implicit scheme:

$$\frac{\mathbf{u}_n - \mathbf{u}_t}{\Delta t} = -\rho^{-1} \nabla p \quad (7)$$

where \mathbf{u}_n is the velocity for next time step. A pressure Poisson equation is then constructed (Chorin and Marsden 1993) by taking divergence of both sides of Eq. 7 and applying divergence-free constraint to velocity field \mathbf{u}_n :

$$\nabla \cdot \mathbf{u}_i = \Delta t \rho^{-1} \nabla^2 p \quad (8)$$

Eq. 8 is discretized using a second-order central difference scheme in the staggered Cartesian grid and solved via a bi-conjugate gradient (BCG) method (Press et al 1992) in PICIN. We note that the boundary conditions are resolved when the Poisson equation is solved. Since staggered Cartesian grid is used in PICIN, it is straightforward to implement free-slip boundary condition for grid-aligned solid boundary. For the free surface boundary, a second-order accurate technique following Gibou et al (2002) is employed to impose a Dirichlet-type condition on the real free surface, whose position is determined by a Signed Distance Field (SDF) constructed via the fast sweeping method (Zhao 2005). Once the pressure field is found, it is then used to project the tentative velocity field onto the nearest divergence free field:

$$\mathbf{u}_n = \mathbf{u}_t - \Delta t \rho^{-1} \nabla p \quad (9)$$

The DLM technique for two-way fluid-solid interaction is also implemented during Eulerian step. A first approximation of solid velocity is acquired by solving Eq.1 and Eq.3 in the solid phase. Once this is done, a density correction within the solid phase is then made via:

$$\mathbf{u}_s = \mathbf{u}_n + \theta \frac{\Delta t}{\rho_s} \mathbf{S}, \quad (10)$$

where:

$$\mathbf{S} = \rho_s \mathbf{A}_c + \rho_s \boldsymbol{\alpha}_c \times \mathbf{r}_i - (\rho_s - \rho) \left\{ \frac{D\mathbf{u}_n}{Dt} - \mathbf{g} \right\}, \quad (11)$$

where θ is the volume fraction of cell part occupied by solid; \mathbf{A}_c and $\boldsymbol{\alpha}_c$ are the translation and rotation accelerations due to collisions between solids and \mathbf{r}_i is the position vector pointing from the solid rotation centre to the cell edges in question. The third term of Eq. 10 accounts for the density difference between solid and fluid. Once the velocity components on cell edges inside the solid phase are corrected, unique velocities are found for the solids by

$$M\mathbf{U} = \int_{\Omega_s} \rho_s \mathbf{u}_s dV, \quad (12)$$

$$I_s \boldsymbol{\omega} = \int_{\Omega_s} \mathbf{r} \times \rho_s \mathbf{u}_s dV, \quad (13)$$

where M and I_s are the mass and moment of inertial of solid objects, respectively. \mathbf{U} and $\boldsymbol{\omega}$ are the unique translation velocity and angular velocity and thus the rigid boundary constraint is enforced. Finally, for each cell edge inside the solid phase, the velocity is given by

$$\mathbf{u}_n = (1 - \theta)\mathbf{u}_s + \theta(\mathbf{U} + \boldsymbol{\omega} \times \mathbf{r}). \quad (14)$$

1.3. The Langrangian step

After the velocity field is updated on the grid, both the velocity and its change are interpolated onto the particles to update the velocity of particles. The particles are then advected through the new divergence-free velocity field, carrying their newly updated velocity via a third-order accurate Runge-Kutta scheme of Ralston (1962). Thus, the advection term of Navier-Stokes equation is integrated with respect to time. We note that the velocity field that particle carries is mapped back to the grid for next step calculation via a kernel function:

$$\mathbf{u}_g = \sum_p \mathbf{u}_p W(x_p - x_g, h) / \sum_p W(x_p - x_g, h) \quad (15)$$

where \mathbf{u}_g and \mathbf{u}_p represent the grid velocity and particle velocity, respectively; W is the cubic kernel function (Liu et al. 2003); h is the kernel length and is usually set equal to 0.7 times of cell length in PICIN.

For more details of this PICIN model, for example, methodologies for extrapolating velocity field from fluid cells to air cells around free surface for particle velocity interpolation, redistributing the particle position and variable time step set up, the reader is recommended to our previous work in Kelly et al. (2014).

2. Validation Case: Sedimentation of Two Solid Particles

The numerical model was validated by modelling the sedimentation of two circular particles and comparing the results with those from Patankar (2001). A 2D tube of 2cm wide (x -direction) and 8cm tall (z -direction) was filled with water ($\nu = 1.0 \times 10^{-6} \text{ m}^2/\text{s}$, $\rho = 1.0 \times 10^3 \text{ kg/m}^3$). The particle had a radius of 0.1cm and density of $1.01 \times 10^3 \text{ kg/m}^3$. At $t = 0\text{s}$, the two particles were placed at heights of 6.8cm and 7.2cm, respectively at the centre of channel and were allowed to fall freely inside water. As the initial distance between the particles

was small, it is known that they will typically undergo drafting, kissing and tumbling (Fortes et al. 1987). For our numerical simulation, the cell size was set at $\Delta x = \Delta z = 0.02\text{cm}$, giving a cell resolution of 100×450 with about 160,000 fluid particles. The time step was set as fixed at $\Delta t = 0.0025\text{s}$.

The collision force between particles and walls was calculated using the method proposed in Glowinski et al. (1999). For the force between particles, the approach can be expressed as:

$$F_{i,j}^p = \begin{cases} 0, & d_{i,j} > R_i + R_j + \lambda \\ \frac{1}{\theta_p} (\mathbf{x}_i - \mathbf{x}_j)(R_i + R_j + \lambda - d_{i,j}), & d_{i,j} \leq R_i + R_j + \lambda \end{cases} \quad (16)$$

where \mathbf{x}_i and \mathbf{x}_j are the centre positions of particles; R_i and R_j are the radius of particles; $d_{i,j}$ is the distance between the centres of particles; λ is the ranging distance that decides when the particles start to exert force on each other (currently set to $1.5\Delta x$ to avoid cells been occupied by different solids at the same time) and θ_p is a stiffness coefficient given as $1.0 \times 10^{-6} \Delta x$ in PICIN. Similar formulate are used for the interaction between particles and walls by placing symmetric ghost particles with respect to the wall.

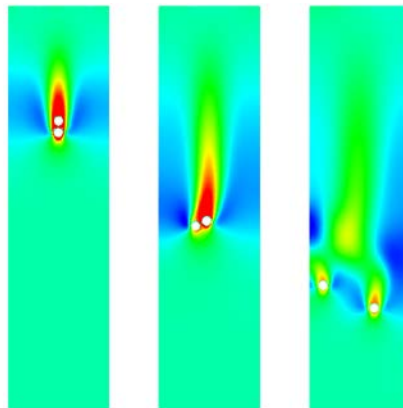


Figure 1 Snapshots of numerical simulation for two particles sedimentation. The colour represents vertical velocity contour scaled from -0.01m/s (blue) to 0.005m/s (red). From left to right, the snapshots show stages of drafting, kissing and tumbling at $t = 1.0\text{s}$, 3.0s and 5.0s .

Figure 1 shows snapshots of the numerical simulation representing the typical three stages. The results are in reasonable agreement with those of Patankar (2001). Figure 2 depicts the comparison of particle velocities between the data from Patankar (2001) and our results. It can be seen that the agreement is good, although some differences are shown. These small differences are expected as different numerical models are used and our model has a free surface boundary on the top.

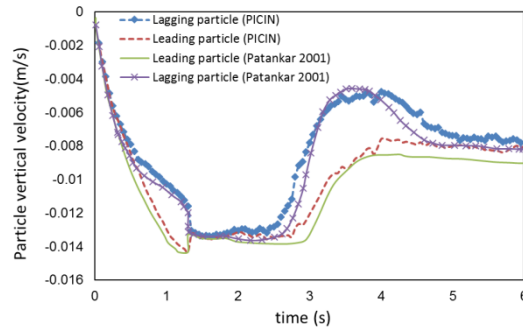


Figure 2 Comparison of particle vertical velocity.

3. Test Case 1: Fall Pipe (Closed Bottom) Rock Dumping

The fall pipe rock dumping case was an extension study of the two particle sedimentation. In this case, 72 solid objects with irregular shapes were initially and randomly placed on the top of the tank just under the free surface. The tank had a width of 1.0m and the solid objects were given an average dimension of 0.2m width. While the same fluid was used as in the particle sedimentation study with a filling depth of 9.8m, the solid density was given uniformly at $2.50 \times 10^3 \text{ kg/m}^3$ which roughly simulates the solid as rocks.

The multiple solid-solid interactions were handled using the collision model of Glowinski et al.(1999) augmented with the multi-sphere DEM approach given in Favier et al.(1999). In particular, the solid object boundary was discretized by small particles with an interval of about $0.2\Delta x$. The single force between small particles of different objects or the tank walls was calculated using the collision model adopted in the validation case above. In addition, a friction force was implemented via the dynamic friction force theory, i.e. $f = \mu F$, where μ was given as 0.65 and F is the single force mentioned above. Overall forces for the objects were then summed up from their discretized particles based on the multi-sphere DEM approach. We note here that the momentum was conserved during the implementation of solid interaction.

Figure 3(a) presents a sketch of the numerical set-up. For this simulation, the cell size was set at $\Delta x = \Delta z = 0.02\text{m}$, resulting in a cell resolution of 52×502 with about 116,000 fluid particles. The CFL number was set at 0.5 to adapt the time step such that no particles move more than one cell at each time step. It took about 5.6hrs for 30 seconds of simulation on an Intel(R) i5-3470 CPU@3.2GHz core.

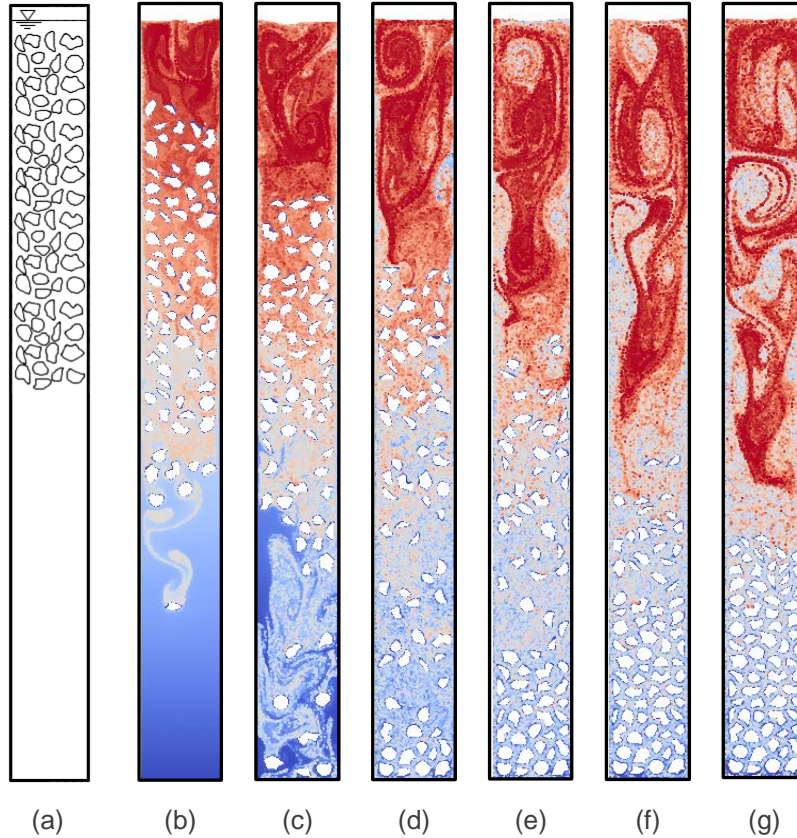


Figure 3 Numerical set up (a) and snapshots (b ~ g) of numerical simulation for rocks falling in pipe. The colour represents the mixing of vertical layers scaled from 0 (cold) to 9.8 (warm) at $t = 5.0s, 10.0s, 15.0s, 20.0s, 25.0s, 30.0s$.

Figure 3(b) ~ Figure 3(g) present snapshots of the numerical simulation at different time instants (5s - 30s). It can be seen that the vertical fluid layers were sufficiently mixed due to the movement of rocks. Also, it is clear that while the leading rock layer quickly hits the bottom of tank, the upper rock layers were slowed down because of the interactions between each other. We note here that the gaps between objects are due to the fact that we have given a ranging distance in Eq. 16 for the interactions between solid objects, which could be reduced if adaptive mesh approaches are used to represent solid phases, for example, adopting the quad-tree mesh for 2D problem.

Figure 4 displays snapshots of the velocity field around leading rock layers of numerical simulation at first few seconds. It is observed that few bigger rocks from the column on the right hand side of the tank moves faster than the average flux, and this creates a wake that causes other rocks to move downward slowly or even move upward compared to the unaffected leading rock. We believe this may be one of the reasons that cause clustering (even clogging) when rocks are falling down through pipes, even though some differences at the wakes are anticipated as the rocks in this 2D numerical experiment have 2D cylindrical layout.

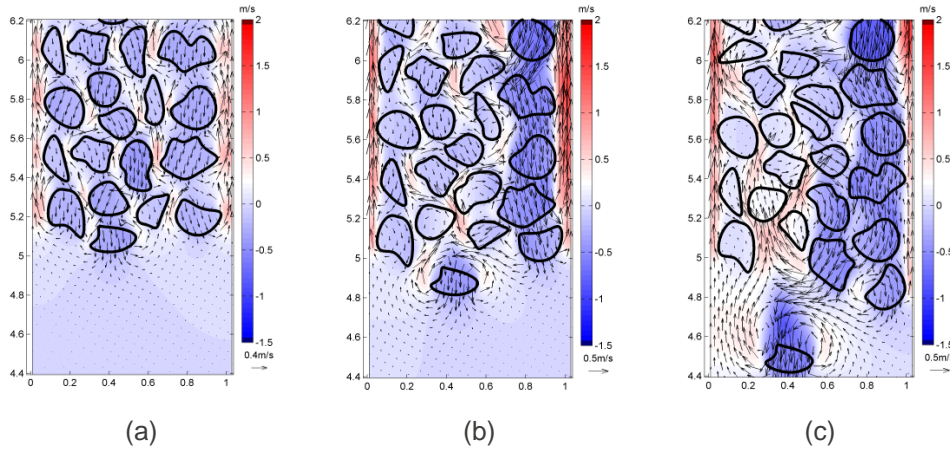


Figure 4 Velocity field around the bottom rocks of numerical simulation at $t = 0.2s, 0.8s$ and $1.6s$. The vectors are plotted out every 5 points based on the grid. The colour represents vertical velocity field

4. Test Case 2: Fall Pipe (Open Bottom) Rock Dumping

For further investigation, we set up an open-bottom pipe model based on the configuration used in Test case 1 and nested it into the centre of an external tank as presented in Figure 5. Two types of open-bottom pipes were studied; the one shown in Figure 5(a) has a continuous, solid wall; the other one as depicted in Figure 5(b) is perforated, with 0.1m wide holes every 1.0m from the open bottom upwards. The external tank was 4.04m wide and filled with 8.8m depth of water. The distance between the bottom of internal pipe and external tank was set at 2.0m. Other numerical settings were kept the same as those used in Test 1.

Figure 6 displays snapshots of numerical simulation for open-bottom full pipe case. As the rocks are accelerated by gravity, there is a pressure increase at the front and pressure decrease at the tail of the rock column and, consequently, the outer free-surface level increases, while the inner level decreases. This results to a reverse pressure gradient inside the pipe. As the free-surface levels oscillate, this reverse pressure gradient oscillates as well and causes a discontinuous fall of the rock columns and eventually a delay of the rock dumping. We note that for the full pipe case it took about 30 seconds of simulation to dump all the rocks from the pipe.

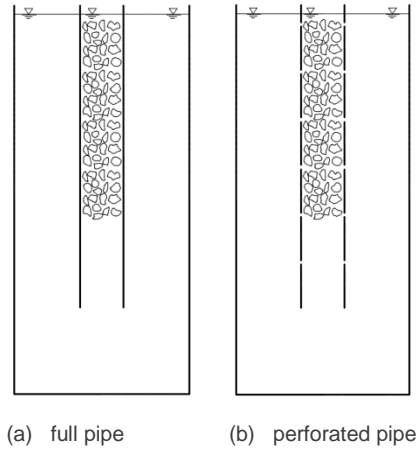


Figure 5 Numerical set up of open-bottom pipe.

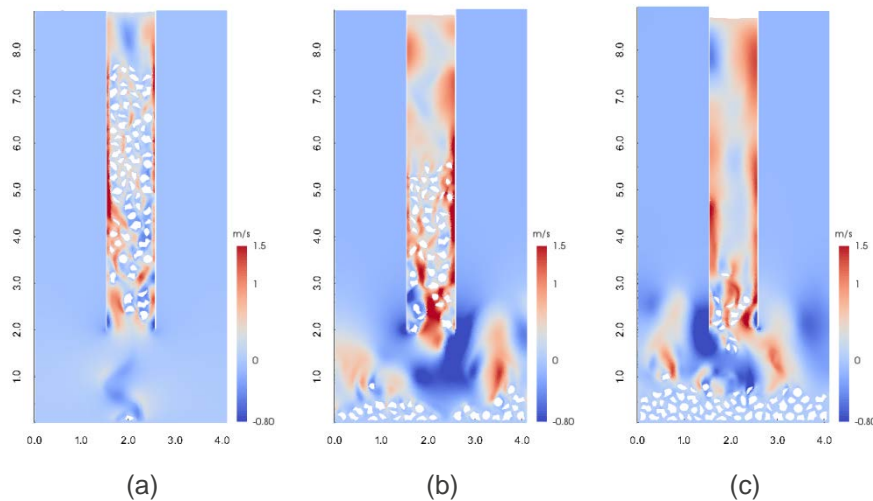


Figure 6 Snapshots of numerical simulation for open-bottom full pipe case at $t = 5.0s, 15.0s$ and $25.0s$. The colour represents vertical velocity field

Figure 7 presents snapshots of simulation for the perforated pipe case. It can be seen that rocks were dumped out very quickly (within about 6s). One of the main reasons is that the reverse pressure gradient does not grow inside the pipe as the existence of holes contribute to the quick equalisation of the pressure at either side of the pipe. The drag induced by the rocks created a flow downwards in the pipe and the speed of each rock was enhanced by the downwards fluid motion. This is typical of the behaviour resulting from semi-open fall-pipes (Beemsterboer 2013).

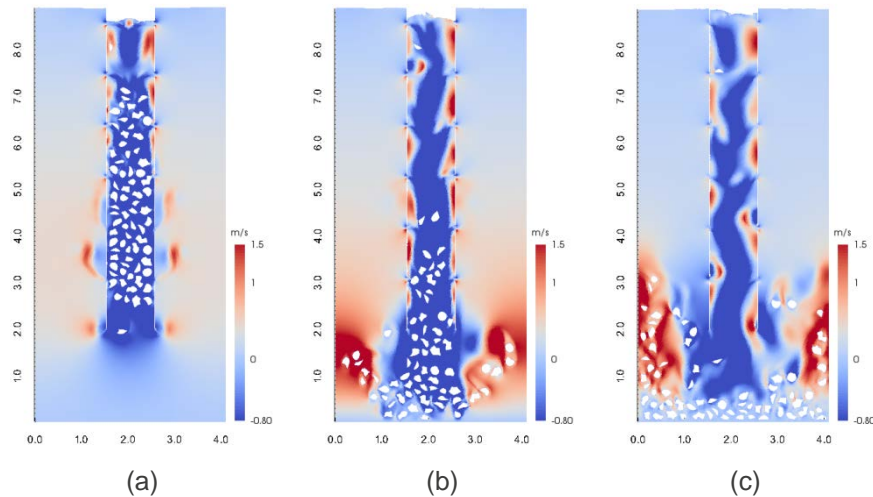


Figure 7 Snapshots of numerical simulation for open-bottom perforated pipe case at $t = 2.0s, 4.0s$ and $6.0s$. The colour represents vertical velocity field.

5. Conclusion

In this work, the PICIN model is used for modelling two-way fluid-solid interaction. The model uses a hybrid Eulerian-Lagrangian method for solving the single-phase incompressible Navier-Stokes equation for free-surface flows. The fluid-solid interaction is implemented using the DLM approach (Patankar 2001). The model is used to simulate the fall of multiple sediment particles in pipes as well as their interaction. The first case is a benchmark case presented that simulates the fall and the interaction of two particles in a 2D pipe; results show good agreement with the ones presented in Patankar (2001). The second case is closer to a realistic scenario, as it models the fall and the interaction of 72 randomly shaped rocks in a fall pipe. The model captures the key elements of the process, including the initiation of rock clustering and effects on productivity of rock dumping. Further work will involve the development of a more realistic fully 3D model.

6. Acknowledgements

The authors acknowledge with thanks the financial support of the University of Bath and HR Wallingford. DMK gratefully acknowledges the support of Florida International University.

7. References

- Beemsterboer, T. N. (2013). "Modelling the immediate penetration of rock particles in soft clay during subsea rock installation, using a flexible fallpipe vessel," Master Thesis for the Technical University of Delft, October 2013.
- Bertho, Y., Giorgiutti-Dauphine, F., Raafat, T., Hinch, E. J., Herrman, H. J., and Hulin, J. P. (2002). "Powder flow down a vertical pipe: the effect of air flow," *J. Fluid. Mech.*, 459, 317-345.

- Chorin, A. J. (1968). "Numerical solution of the Navier-Stokes equations," *Math. Comput.*, 22, 745-762.
- Favier, J. F., Abbaspour-Fard, M. H., Kremmer, M., and Raji, A. O. (1999). "Shape representation of axis-symmetrical, non-spherical particles in discrete element simulation using multi-element model particles," *Engineering Computations*, 16, 467-480.
- Fortes, A. F., Joseph, D. D., and Lundgren, T. S. (1987). "Nonlinear mechanics of fluidization of beds of spherical particles," *Journal of Fluid Mechanics*, 177, 467-483.
- Gibou, F., Fedkiw, R. P., Cheng, L.-T., and Kang, M. (2002). "A second-order-accurate symmetric discretization of the Poisson equation on irregular domains," *J. Comp. Phys.*, 176, 205-227.
- Glowinski, R., Pan, T. W., Hesla, T. I., and Joseph, D. D. (1999). "A distributed lagrange multiplier/fictitious domain method for particulate flows," *International Journal of Multiphase Flow*, 25, 755-794.
- Harlow, F. H., and Welch, J. E. (1965). "Numerical calculation of time dependent viscous incompressible flow of fluid with free surface," *Physics of Fluids (1958-1988)*, 8(12), 2182-2189.
- IADC (2012). "Facts About Subsea Rock Installation, An Information Update from the IADC," Number 3. [<http://www.iadc-dredging.com/ul/cms/fck-uploaded/documents/PDF%20Facts%20About/facts-about-subsea-rock-installation.pdf>]. [Accessed 21/01/2015].
- Kelly, D. M., Chen, Q., and Zang, J. (2014). "PICIN: A particle-in-cell solver for incompressible free surface flows with two-way fluid solid coupling," *Under consideration for publication in SIAM Journal on Scientific Computing (SISC)*.
- Liu, M. B., Liu, G. R., and Lam, K. Y. (2003). "Constructing smoothing functions in smoothed particle hydrodynamics with applications," *Journal of Computational and Applied Mathematics*, 155(2), 263-284.
- Nakahara, A. and Isoda, T. (1997). "1/fa density fluctuation at the slugging transition point of granular flows through a pipe," *Physical Review E*, 55(4), 4264-4273.
- Patankar, N.A., Singh, P., Joseph, D.D., Glowinski, R. and Pan, T.-W. (2000). "A new formulation of the distributed Lagrange multiplier/fictitious domain method for particulate flows," *Int. J. Multiphase Flow*, 26, 1509-1524.
- Patankar, N. A. (2001). "A formulation for fast computations of rigid particulate flows," *Center for Turbulence Research Annual Research Briefs*, 185-196.
- Press, W., Teukolsky, S., Vetterling, W., and Flannery, B. (1992). "Numerical Recipes in Fortran 77: The Art of Scientific Computing," 933 p.
- Raafat, T., Hulin, J. P., and Herrman, H. J. (1996). "Density waves in dry granular media falling through a vertical pipe falling," *Physical Review E*, 53, 4345-4350.
- Ralston, A. (1962). "Runge-Kutta methods with minimum error bounds," *Mathematics of computation*, 16, 431-437.
- Ravelli, F. D. C. (2012). "Improving the efficiency of a flexible fallpipe vessel," Master Thesis for the Technical University of Delft, April 2012.
- Zhao, H. (2005). "A fast sweeping method for eikonal equations," *Mathematics of computation*, 74(250), 603-627.